ACS OMEGA

Article

Cite This: ACS Omega 2018, 3, 55−62

Tough and Variable-Band-Gap Photonic Hydrogel Displaying Programmable Angle-Dependent Colors

Md. Anamul Haque,[†,∥] Kei Mito,[‡] Takayuki Kurokawa,[†,§] Tasuku Nakajima,[†,§] Takayuki Nonoyama,[†,§] Muhammad Ilyas,[‡] and Jian Ping Gong*[,†,§]

[†]Faculty of Advanced Life Science, [‡]Graduate School of Life Science, and [§]Global Station for Soft Matter (GI-CoRE), Hokkaido University, North 21 West 11, Kita-ku, Sapporo 001-0021, Japan

[∥]Department of Chemistry, University of Dhaka, Nilkhet Road, Dhaka 1000, Bangladesh

Supporting Information

ABSTRACT: One-dimensional photonic crystals or multilayer films produce colors that change depending on viewing and light illumination angles because of the periodic refractive index variation in alternating layers that satisfy Bragg's law. Recently, we have developed multilayered photonic hydrogels of two distinct bulk geometries that possess an alternating structure of a rigid polymeric lamellar bilayer and a ductile polyacrylamide (PAAm) matrix. In this paper, we focus on fabrication of composite gels with variable photonic band gaps by controlling the PAAm layer thickness. We report programmable angle-dependent and angle-independent structural colors produced by composite hydrogels, which is achieved by varying bulk and internal geometries. In the sheet geometry, where the lamellae are aligned parallel to the sheet surface, the photonic gel sheet exhibits strong angle-dependent colors. On the other hand, when lamellae are coaxially aligned in a cylindrical geometry, the gel rod exhibits an angle-independent color, in sharp contrast with the gel sheet. Rocking curves have been constructed to justify the diverse angle-dependent behavior of various geometries. Despite varying the bulk geometry, the tunable photonic gels exhibit strong mechanical performances and toughness. The distinct angle dependence of these tough photonic materials with variable band gaps could benefit light modulation in displays and sensor technologies.

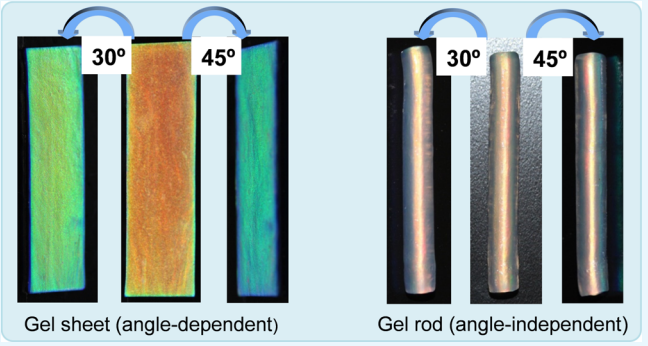

INTRODUCTION

Photonic hydrogels, which possess a three-dimensional polymer network structure with periodic variations of refractive index, are potential candidates for soft and tactile displays, sensor systems, packaging, and advertising.[1−10] The ordering present in these soft hydrogels causes them to exhibit a "structural color" that can be reversibly tuned by varying the periodic spacing through external stimuli such as stress,[11−14] temperature,[15−18] pH,[19,20] and solvent exchange[21−23] or by varying the refractive index of the material.[24] Therefore, photonic hydrogels are promising materials for displays and sensors through utilizing stimuli-responsive structural colors rather than requiring colored filters or additional optical elements.[2] The structural color of materials that possess one-dimensional photonic crystal structures or multilayer films[8,25] shows distinct variations depending on viewing and light illumination angles. In contrast, amorphous photonic structural arrays are responsible for viewing-angle-independent colors.[8] Angle-dependent continuous color filtering allows the multicolor appearance of see-through organic photovoltaics[26] and plasmonic chips for the construction of reflection-based spatial light modulators.[27] On the other hand, changes in color associated with viewing or illumination angle variation can also pose major challenges for the development of full-color displays with wide viewing angles.[8,24] Therefore, both tunable angle-dependent and angle-independent colors in photonic materials are high in demand for optical devices. Researchers, to date, have shown that materials having a short-range order in periodic structures display angle-independent colors originating from a wavelength-specific constructive interference in the visible region.[28−30] Structurally colored materials that exhibit angle-dependent colors most likely possess long-range periodic structures.[31−33] Takeoka reported angle-dependent colors by constructing colloidal crystalline arrays and angle-independent colors by assembling colloidal amorphous arrays.[8] To the best of our knowledge, tuning between angle-dependent and angle-independent colors by modifying the photonic nanostructure in line with the bulk geometry has rarely been reported.

On the basis of long-range periodic lamellar structures, we have recently developed a tough photonic hydrogel that exhibits tunable colors through various stimuli including stress, temperature, and pH.[34−40] The photonic hydrogel consists of

Received: October 11, 2017
Accepted: December 20, 2017
Published: January 4, 2018

DOI: 10.1021/acsomega.7b01443
ACS Omega 2018, 3, 55−62

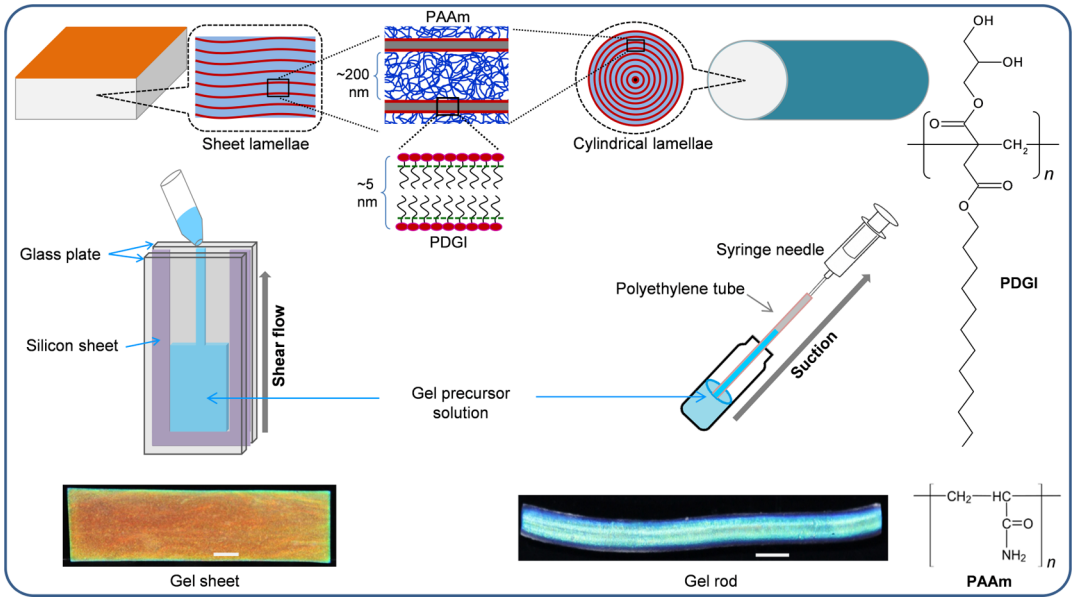

Figure 1. Schematic illustrations, preparation methods, and photographs of photonic hydrogel sheets (left) and rods (right). The photonic hydrogel consists of self-assembled bilayers (several-nanometer thick) of PDGI and ductile PAAm layers (few-hundred-nanometer thick). PDGI/PAAm gel sheets were prepared by applying shear flow of the precursor solution between two parallel glass plates prior to polymerization. On the other hand, gel rods were fabricated by using suction to incorporate the precursor solution into a polyethylene tube. PDGI bilayer sheets are aligned parallel to the glass substrates for gel sheets and coaxially to the cylindrical tubes for gel rods. The scale bars are ~2 mm.

an alternate packing of rigid polymeric bilayers [self-assembly of amphiphilic poly(dodecyl glyceryl itaconate) (PDGI)] and ductile polyacrylamide (PAAm) layers (Figure 1). Long-range periodic photonic structures have been fabricated by shear-induced orientation of dodecyl glyceryl itaconate (DGI) bilayer domains during preparation. A gel precursor solution containing DGI monomers undergoes self-assembly to form lamellar bilayers that can be aligned along the shear direction. Given this ability, long-range ordering of lamellar bilayers can be controlled by the geometry of the reaction cell, which determines the shear flow of the precursor solution during injection. When the precursor solution is injected into a rectangular reaction cell consisting of two parallel glass plates, lamellar bilayers are aligned parallel to the glass wall. Upon UV curing, hydrogel sheets are formed, where lamellar bilayers uniaxially appeared along the sheet surface and trapped between PAAm matrices (Figure 1, left). On the other hand, rod-shaped hydrogels, in which bilayers form a concentric multicylindrical packing, have been achieved by applying suction to a precursor solution into a cylindrical polyethylene tube (Figure 1, right).

Herein, we report the fabrication of composite hydrogels (PDGI/PAAm) with variable photonic band gaps and the resulting angle-dependent or angle-independent structural colors based on the specific photonic nanostructure and bulk gel geometry. Gel sheets and rods of varying photonic band gaps within the visible spectrum were fabricated by controlling the swelling degree of the PAAm matrix. Photonic gel rods exhibited angle-independent colors, in sharp contrast to gel sheets, which showed strong angle dependence. The contrasting angle dependence of both the gels is characterized by constructing rocking curves and comparing their lamellar geometries. Despite various bulk geometries with a distinct lamellar packing, both the gels are soft and ductile, exhibiting high mechanical strength and toughness. Understanding the relationship between the photonic nanostructure and the angle dependence of these soft and tough hydrogels could impact the material design for light modulation, visualization, optical sensing, and display technologies.

RESULTS AND DISCUSSION

Photonic hydrogel sheets possess several thousands of rigid PDGI lamellar bilayers stacked periodically into a soft and ductile PAAm matrix. PDGI lamellae are entrapped in a chemically cross-linked PAAm network by one-step polymerization in the presence of a small amount of a chemical cross-linker. In the as-prepared state, gel sheets [0.1 M DGI, 2.0 M acrylamide (AAm), and 0.1 mol % *N*,*N*′-methylenebis-(acrylamide) (MBAA) of AAm] are almost transparent and exhibit a pale violet color (Figure S1). However, visible colors appeared depending on the swelling degree in pure water. PDGI bilayers are impermeable to water and other hydrophilic molecular species. Because of the uniaxial orientation of the PDGI bilayers, the water-permeable PAAm network can swell freely in the direction perpendicular to the bilayers and the bulk thickness of the gel sheet almost doubled. The swelling is related to the increase in the PAAm layer thickness and a corresponding increase in the inter-bilayer distance *d*, which leads to a red shift in the gel color. The thickness of a single PDGI bilayer (d_{PDGI}) was reported in the literature previously as ~4.7 nm.[41] Therefore, the thickness of each PAAm layer (d_{PAAm}) can be estimated from *d*. d_{PAAm} of the water-swollen gel sheet, which exhibits an orange-red color, is estimated as ~250 nm. At room temperature, the single PDGI bilayer membrane is rigid with a modulus on the order of several megapascals and the PAAm matrix is soft with a modulus of few kilopascals.[34,39] The refractive index of a PDGI bilayer membrane is considered to be that of a lipid bilayer, which is reported in the range of 1.42−1.45.[42] The refractive index of a PAAm layer is considered to be ~1.33 (the refractive index of water) as it contains mostly water (98%).[43] Therefore, the PDGI/PAAm composite gel exhibits visible colors at various wavelength

DOI: 10.1021/acsomega.7b01443
ACS Omega 2018, 3, 55−62

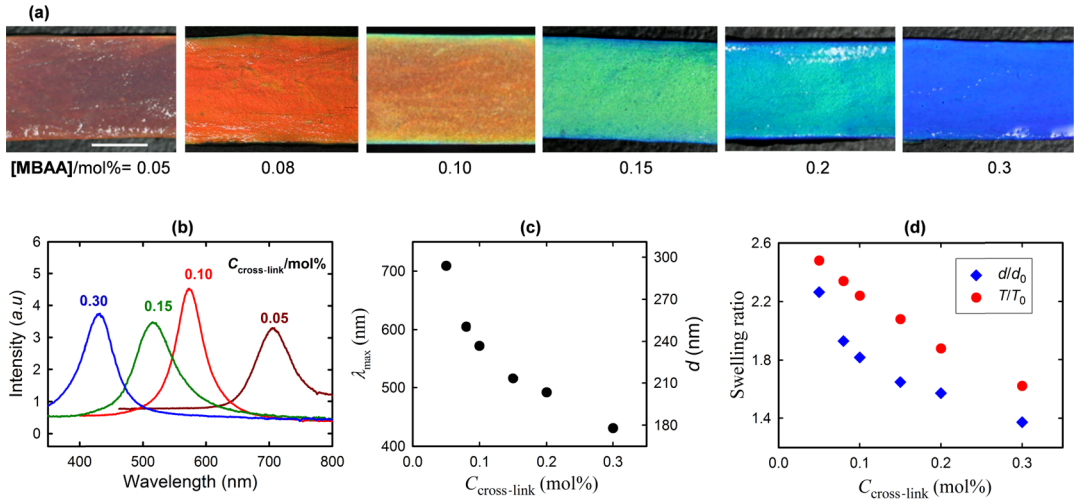

Figure 2. (a) Photographs of the gel sheets prepared at various cross-linker concentrations (MBAA) show a blue shift with an elevated MBAA content. (b) Reflection spectra of the gels are measured at various cross-linker concentrations. Both incident and detection angles (θ) were set at 60° for the spectra measurements. (c) Wavelength of maximum intensity (λ_{max}) and interlamellar distance (d) are plotted as a function of cross-linker concentration. d was calculated from λ_{max} using Bragg's law, $2nd \sin\theta = m\lambda$, where n, d, θ, m, and λ are the refractive index of water, periodic lamellar spacing, Bragg's angle, diffraction order, and wavelength of diffracted light, respectively. (d) Bulk swelling ratio of gel thickness (T/T_0) and d-ratio (d/d_0) are shown as a function of cross-linker concentration, where T_0 and d_0 and T and d stand for the reference state (as-prepared) and swollen state, respectively, of gels with various cross-linking densities. Cross-linker concentrations are expressed as mol % with respect to AAm molar concentrations. The scale bar is ∼5 mm.

bands because of the periodic refractive index variation of alternating layers that satisfy the Bragg's law for diffraction of visible light.

The periodic lamellar spacing, d, of the gel sheets and correspondingly their color can be tuned by varying the DGI concentration during preparation, mechanical stress, and so forth.[34] In this work, d was varied by regulating the PAAm layer thickness. This was achieved by controlling the swelling degree of the PAAm matrix. The PDGI/PAAm gel sheets were prepared at various cross-linking concentrations using MBAA as a cross-linker in the PAAm network. The photographs of the gel sheets prepared with various MBAA concentrations are shown in Figure 2a. With increasing MBAA concentration, a blue shift is observed in accordance with the corresponding reflection spectra, as shown in Figure 2b. The wavelength of maximum intensity (λ_{max}) and bilayer spacing (d) decrease accordingly (Figure 2c). Therefore, a shift in the gel color is attributed to the decrease in d. At a high cross-linking density, the swelling degree of the PAAm matrix was reduced, which resulted in a decrease in d. The bulk swelling ratio along the thickness of the gel (T/T_0) also decreased in accordance with the d-ratio (d/d_0) (Figure 2d), where T_0 and d_0 and T and d are the reference states (as-prepared) and swollen states, respectively, for gels with various cross-linking concentrations.

The gel rods were prepared with compositions identical to those of the gel sheets (0.1 M DGI, 2.0 M AAm, and 0.1 mol % MBAA of AAm), resulting in an almost transparent gel that exhibits a pale violet color in the as-prepared state (Figure S1). However, the gel rods with a preparation composition identical to that of the gel sheets appear greenish-blue after swelling in water. The difference in color between swollen gel sheets and rods is due to the swelling process. The gel sheets swelled in the thickness direction by a factor of more than 2, whereas the gel rods swelled in the diameter direction by less than a factor of 2.[34,36] The bilayer spacing, d, of the gel rods can also be varied by controlling the swelling degree of the PAAm layer, which is achieved by varying the concentrations of the cross-linker. The gel rod exhibits a blue shift, similar to the gel sheet, at higher MBAA concentrations (Figure 3a). The swelling ratio of the gel rod in the diameter direction (D/D_0) decreased with increasing MBAA concentration, indicating a decrease in d as a result of the reduced swelling of the PAAm matrix.

The flat periodic lamellar structures in the gel sheets were previously confirmed by various techniques.[34,39] In the present work, polarizing optical microscopy (POM) images are shown to justify the contrasting microstructure of both flat (gel sheet) and cylindrically symmetric (gel rod) lamellar structures (Figure 4). The gel sheets were observed under cross-polarizers in the presence of a tint plate (530 nm) using POM (Figure 4a). In the cross-sectional view at 0° to the polarizer, the POM image appears magenta (Figure 4a(i)). However, the images show orange (Figure 4a(ii)) and blue (Figure 4a(iii)) interference colors at −45° and +45° rotations, respectively. These results indicate monodomain lamellar bilayers in parallel to the top surface of the gel sheets. The top-view images, which show solid magenta colors for all sample angles, indicate no in-plane alignment, further justifying the in-plane flat lamellae (Figure 4a(iv−vi)).

The rod-shaped gel was also observed under cross-polarizers from the top as well as from a cross-sectional view (Figure 4b). POM images, which were taken from the cross-section of the rod in the presence (Figure 4b(i)) and absence (Figure 4b(ii)) of a tint plate, show a Maltase cross, which clearly indicates a concentric alignment of bilayers along the periphery of the rod. Large-scale concentric cylindrical lamellae of the gel rods were further revealed by the POM images taken perpendicular to the long axis of the rod. POM produces completely dark images over the whole sample when the long axis of the rod was positioned in the polarizer direction (Figure 4b(iii)). However, at −45° and +45° rotations, orange and blue birefringences were observed, respectively, together with a thin line of magenta color in the center along the long axis (Figure 4b(iv,v)). These birefringence micrographs clearly justify the

DOI: 10.1021/acsomega.7b01443
ACS Omega 2018, 3, 55−62

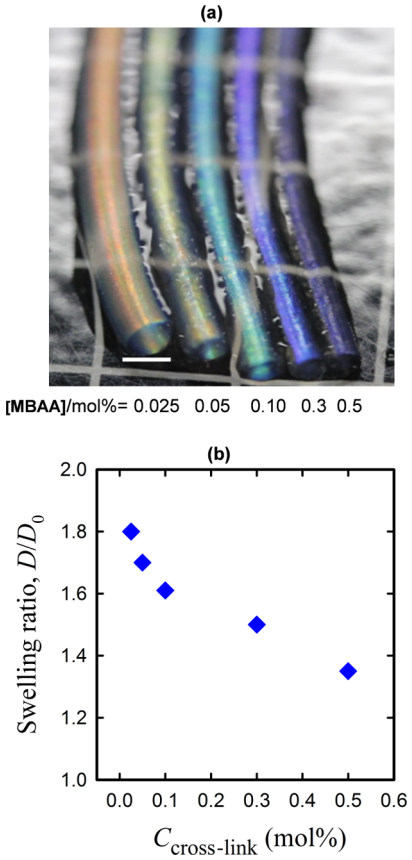

Figure 3. (a) Photographs of gel rods prepared at various cross-linker concentrations (MBAA) show a blue shift at a higher MBAA content. (b) Gel rod bulk swelling ratios in the diameter direction (D/D_0) decrease with increasing cross-linker concentration. The scale bar is ~2 mm.

existence of large-scale cylindrical lamellae with a concentric alignment in the gel rods.

Although the gel sheets and rods possess a distinct bulk geometry as well as internal nanostructured packing, they exhibit comparable mechanical strength and toughness (Figure 5). Both the gels possess a modulus of ~100 kPa and a work of extension on the order of several MJ m^{-3}.

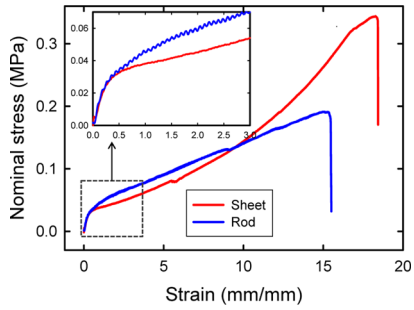

Figure 5. Nominal stress vs strain curves of a gel sheet and a gel rod indicate comparable levels of mechanical properties. The modulus of both the gels is ~100 kPa. Compositions of these two gels at preparation are identical (0.1 M DGI, 2.0 M AAm, and 0.1 mol % MBAA of AAm). The deformation velocity was 200 mm/min.

To observe the angle dependence of the structural color, real-time movies and photographs of both gel sheets (0.1 mol % MBAA) and rods in the red photonic band (0.025 mol % MBAA) were taken at different viewing angles (Figure 6a,b and Movies S1 and S2). The gel sheet exhibits an orange-red color at a viewing angle of 0°. The color changes from red to blue with increasing viewing angle on both directions (±30, ±45, and ±60°) (Figure 6a). This angle-dependent behavior is similar to some natural phenomena such as soap bubbles, beetle's exoskeletons, and bird's feathers.[44−46] The gel rods, which possess an orange-red color at 0°, do not undergo any noticeable shift in color by changing the viewing angle in both directions, which is in sharp contrast to the sheets (Figure 6b and Movie S2). It should be noted here that we chose gel rods of different preparation conditions (0.025 mol % MBAA) to

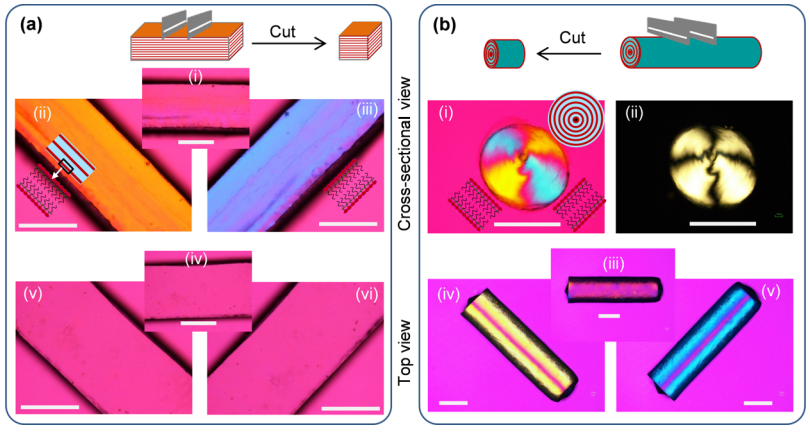

Figure 4. POM images of gel sheets (a) and rods (b). All of the images are taken under cross-polarizers in the presence of a tint plate (530 nm) [except for b(ii)]. The birefringence of the samples is assigned to the monodomain bilayers and elongated PAAm chains because of the anisotropic swelling. [a(i−iii)] Cross-sectional images of a gel sheet at 0° to the polarizer (i) appear magenta but orange at −45° (ii) and blue at +45° (iii), indicating uniaxially aligned lamellae parallel to the top surface of the gel. [a(iv−vi)] Top-view POM images of the gel sheet show only magenta color at all angles when the sample stage is rotated, which indicates no in-plane sheet lamellae. [b(i,ii)] Images taken from the cross-section of the gel rod in the presence (i) and absence (ii) of a tint plate show a Maltese cross, which clearly indicates the concentric alignment of lamellae to form a multicylindrical packing. [b(iii−v)] Images taken perpendicularly to the long axis of the rod (top view) are completely magenta (iii) over the whole sample when placed at 0° to the polarizer but orange (iv) and blue (v), separated by a solid magenta line, when placed at −45° and +45°, respectively. This further indicates a large-scale concentric cylindrical alignment of lamellae in the gel rods. The scale bars are 1.0 mm.

DOI: 10.1021/acsomega.7b01443
ACS Omega 2018, 3, 55−62

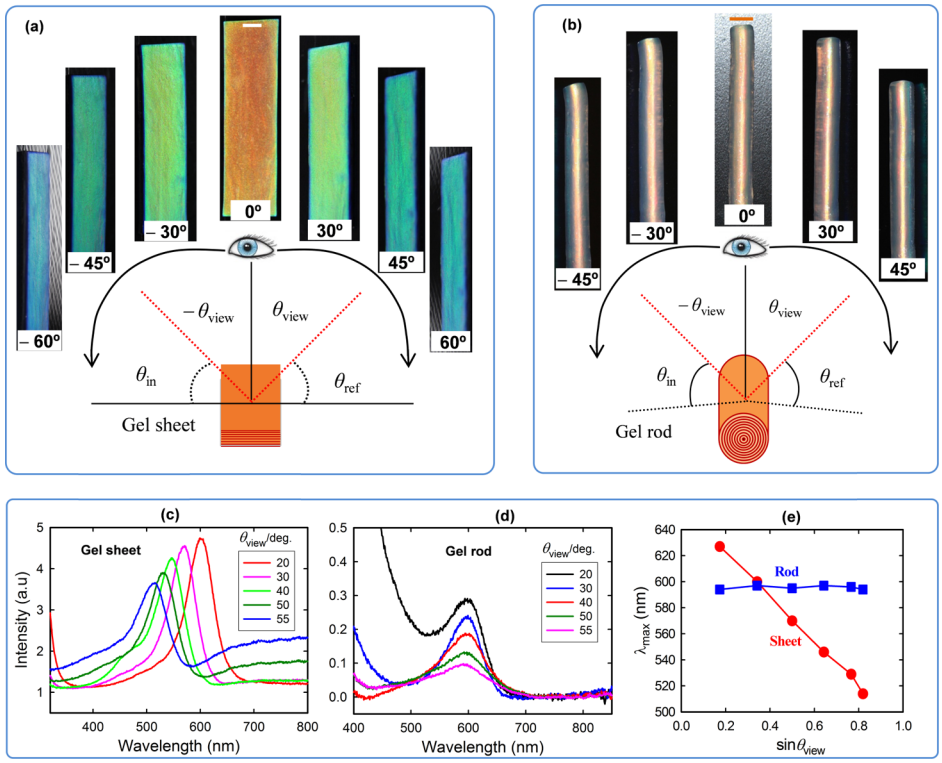

Figure 6. Viewing angle dependence of lamellar gels with different geometries. (a) Photographs of gel sheets taken at various viewing angles in both directions show a blue shift. (b) Photographs of gel rods taken at various viewing angles in both directions exhibit no significant change in color. Reflection spectra of the sheets (c) and rods (d) taken at various viewing angles (θ_{view}) while keeping the incident (θ_{in}) and reflection (θ_{ref}) angles identical to 90 − θ_{view} (θ_{in} = θ_{ref} = 90 − θ_{view}). The reflection peak of the gel sheets shifts from red to blue, but that of the rods remains almost unchanged with increasing viewing angle. (e) Change of λ_{max} with the viewing angle for both gel sheets and rods. The scale bars are 2.0 mm.

achieve a color identical to that of the gel sheet for the angle-dependent study. Although long-range, flat multilayer structures produce high angle dependence in the case of gel sheets, rods with cylindrical lamellar structures exhibit negligible angle dependence, which is analogous to the structural color in *Morpho* butterflies that show no angle dependence.[24]

The reflection spectra of both gel sheets and rods were measured at various viewing angles using an angle-measuring reflection apparatus. During the measurement, incident (θ_{in}) and reflection (θ_{ref}) angles were identical, where θ_{in} = θ_{ref} (=90 − θ_{view}), where θ_{view} is the viewing angle. The reflection spectra of the gel sheets showed a blue shift in the peak wavelength (Figure 6c), whereas the peak wavelength of the rods does not change with increasing θ_{view} (Figure 6d), which is in consistence with their appearance. The wavelength at maximum intensity (λ_{max}) for both the gels was plotted as a function of θ_{view} and is demonstrated in Figure 6e. A large shift in the peak wavelength (~120 nm) is observed for the gel sheet by changing the viewing angle from 10 to 55°. In contrast, no significant change in λ_{max} for the gel rod is observed. However, the peak intensity of the gel rod is much lower than that of the sheet geometry. The angle dependence of the gels is related to Bragg's law, $2nd \sin\theta = m\lambda$, where n, d, θ, m, and λ are the refractive index of water, periodic lamellar spacing, Bragg's angle, diffraction order, and wavelength of diffracted light, respectively.[47−49] As the sheet geometry possesses flat lamellae, the Bragg's angle (θ) is equivalent to θ_{in} or (90 − θ_{view}). According to Bragg's law, lower wavelength light is reflected at a smaller Bragg's angle, which is why a blue shift occurred in the gel sheet when observed at a higher viewing angle. On the other hand, because the rod geometry possesses cylindrical lamellae, incident/reflected light impinges on the circular lamellar surface at various angles. Although the viewing angle is changed spatially, the true angle of incidence and reflection with respect to the sample position remains unchanged. Therefore, the phenomena of Bragg's diffraction do not vary upon rotation of the cylindrical lamellar gel. Regardless of the sample position or viewing angle, incidence and reflection always appeared at an angle of 90° on cylindrical lamellae for the gel rods.

To quantitatively characterize the angle dependence, we further construct rocking curves where the incident (θ_{in}) and detected (θ_{ref}) beams with respect to the initial position of samples were set in such a way that the angle between the incident and detected beams (ω) remains fixed upon rocking the sample (Figure 7a,b). Keeping ω = 50°, both the gel samples were rocked at various angles (ψ).

The reflection spectra of both gels taken at various rocking angles are shown in Figure 7c,d. The reflection peak intensity of the gel sheet falls sharply by rocking the sample at a small angle of only ~10°, whereas a negligible change in the peak intensity is noticed for the rod while rocking even at an angle of 30°. The rocking curves, intensity ratio (I/I_0) versus rocking angle, for both gels are plotted, where I and I_0 are the reflection peak intensities at various rocking angles and at zero rocking angle, respectively (Figure 7e). A sharp rocking impact is apparent for the gel sheets, whereas a broad impact can be seen for the rods. The maximum intensity observed at 0 rocking angle for the gel sheet confirms that lamellar bilayers are mostly aligned parallel to the top surface. In the case of the gel rods, the angle of the incident beam and detector remained unchanged with respect to the sample position regardless of the rocking angle, indicative of angle-independent structural colors. With the gel

DOI: 10.1021/acsomega.7b01443
ACS Omega 2018, 3, 55−62

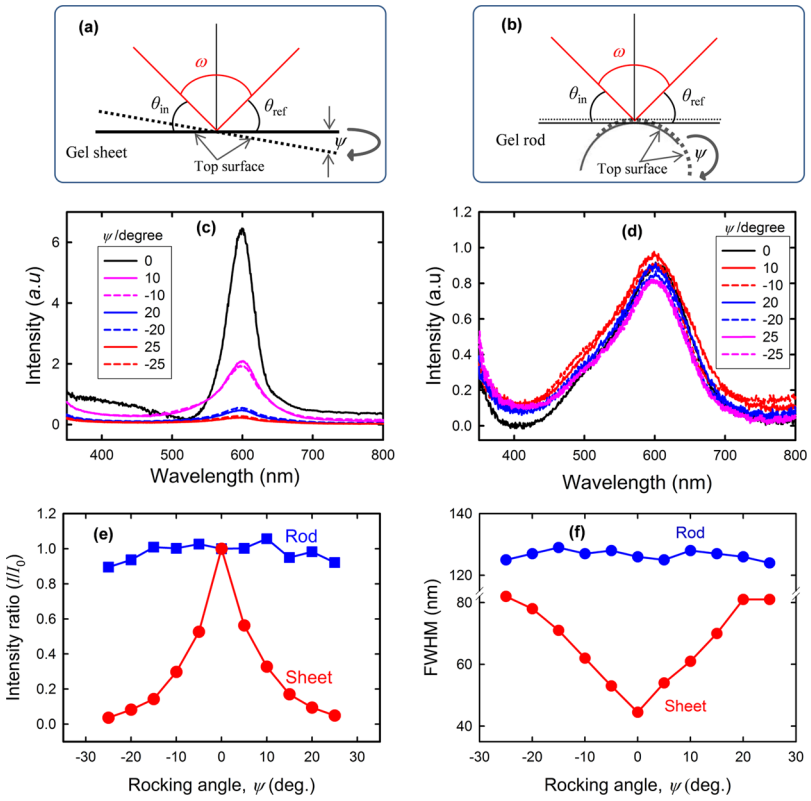

Figure 7. Schematic representation of the reflection spectra measurement when the gel sheets (a) and rods (b) were rocked at different angles (ψ). Reflection spectra of the gel sheet (c) and rod (d) taken at various rocking angles (ψ). A significant decrease in the peak intensity, even at small rocking angles, for the gel sheet was noticed, whereas the peak intensity for the gel rod is almost independent of the rocking angle. (e) Rocking curves, a plot of intensity ratio (I/I_0) vs rocking angle, for both the sheet and rod geometries, where I and I_0 represent the reflection peak intensities at various rocking angles and at 0 rocking angle, respectively. The angle between the incident beam and reflected light, ω, was kept constant at 50°. (f) Full width at half-maximum (fwhm) for the gel sheets and rods is also plotted as a function of rocking angle.

sheet, the incident and detection angles with respect to the sample position always change with varying rocking angle, demonstrating highly angle-dependent structural colors. Similar results were obtained when the angle, ω, between the incident and reflected beams is varied for both gels (Figure S2). Full width at half-maximum (fwhm) for both gels is also plotted as a function of rocking angle in Figure 7f. The bilayer undulation in the gel sheet may affect its rocking intensity distribution, whereas there is negligible influence on rocking for the gel rod. Therefore, the rocking curves clearly confirmed the distinct angle dependence of both gels.

The distinct angle-dependent behavior has been previously demonstrated by constructing colloidal crystalline arrays or by assembling colloidal amorphous arrays.[8] These photonic systems are isotropic on the macroscale and have limited applications because their structure rarely influences their mechanical performances. Although rolled-up multilayered photonic fibers[25] show moderately improved mechanical functions, they exhibit only angle-independent colors. On the other hand, our photonic gel system is anisotropic (on both the macro- and microscales) and exhibits excellent mechanical functions as well as color tunability and promising optical occurrences by modifying the external geometry along with the internal photonic nanostructure. Moreover, our photonic system could guide us to understand the unique optical occurrences in nature as well as various biological organisms, such as soap bubbles, beetles, fishes, cuticles, butterflies, and some types of bird feathers.

CONCLUSIONS

Photonic hydrogels with tunable angle-dependent structural colors have been developed, which is achieved by varying the bulk geometry and their photonic nanostructures. Hydrogel sheets with uniform lamellar domains exhibit strong angle-dependent structural colors, whereas gel rods with concentric cylindrical lamellae show angle-independent colors, in sharp contrast to the sheet geometry. Rocking curves have been constructed to justify the diverse angle dependence of lamellar photonic hydrogels with various bulk geometries. Both gel sheets and rods with variable photonic band gaps have been fabricated by varying the swelling degree of the PAAm layer. Despite varying the bulk geometry, softness, and ductility, both gels exhibit high mechanical performances and toughness. Owing to the soft and tough nature of these materials, stimuli-responsive photonic band gap, and distinct angle dependence, these promising photonic nanocomposite materials could be potentially useful in display technologies and to uncover unique optical occurrences in nature.

EXPERIMENTAL SECTION

Materials. An amphiphilic monomer, DGI (n-$C_{12}H_{25}$–$OCOCH_2C(=CH_2)COOCH_2CH(OH)CH_2OH$), was synthesized following the procedure described earlier.[34] After completion of two-step reactions, the crude product was purified at least twice by a silica gel column (silica gel 60 N, Kanto Chemical Co., Inc.). The DGI fraction was eluted with a hexane/ethyl acetate mixture (1:1 by volume) and was further

DOI: 10.1021/acsomega.7b01443
ACS Omega 2018, 3, 55−62

purified twice by recrystallization from an acetone/hexane mixture (1/1 by weight). MBAA was recrystallized from ethanol, AAm was recrystallized from chloroform, and Irgacure 2959 and sodium dodecyl sulfate (SDS) were used as received. Millipore deionized water was used to prepare the monomer solutions and for the swelling of the gel.

Preparation of Gel Sheets and Rods. PDGI/PAAm gel sheets and rods were prepared by simultaneous free-radical polymerization from an aqueous solution of 0.1 M DGI, 0.025 mol % SDS of DGI, 2 M AAm, 0.025−5.0 mol % MBAA of AAm as a cross-linker, and 2 mM Irgacure as an initiator.[34,36] The precursor solution was prepared by mixing all components which contained random microdomains of self-assembled DGI lamellar bilayers dispersed in an AAm solution. Gel sheets with flat lamellar bilayer structures parallel to the sheet surface were fabricated by applying shear flow of an equilibrated precursor solution between two parallel glass plates. Prior to polymerization, the precursor solutions were injected in a rectangular-shaped glass mold (100 × 10 × 0.5 mm^3) at a shear rate of ∼200 s^{-1}, where the two parallel glass plates were separated by a 0.5 mm thick silicon spacer (Figure 1, left). Because of the strong shear flow between the two parallel glass plates, random lamellar bilayer domains were aligned in the direction parallel to the glass substrate. After 8 h of UV polymerization, uniform, flat lamellae were stacked periodically and entrapped in a chemically cross-linked PAAm matrix to create the hydrogel sheet. On the other hand, PDGI/PAAm gel rods were fabricated by using a polyethylene tube (1.0 mm diameter and 200 mm long) as a reaction cell to apply strong shear flow along the axial direction of the tube (Figure 1, right). The gel precursor solution was prepared in the same manner as above. One end of the tube was immersed in the precursor solution, and the other end was connected to a syringe. Suction was applied to the precursor solution at a high speed (shear rate > 200 s^{-1}) until the tube was filled. Under strong shear flow, random lamellar domains in the precursor solution were oriented along the wall of the tube to form multicylinder lamellae. The rod structure was stabilized in the PAAm matrix after 8 h of UV polymerization. Both gels were immersed in water to achieve an equilibrium swollen state.

Reflection Spectra Measurements. Variable angle reflection measurement optics (Hamamatsu Photonics K.K., C10027A10687) were used for exposing the gels to white light and detecting the reflected light. A xenon lamp was used as a light source to measure the reflection spectrum. A photonic multichannel analyzer (Hamamatsu Photonics K.K., C10027) was used for analyzing the detected signal. To observe the angle-dependent color, the reflection spectra of the gel samples were measured at various viewing angles (θ_{view}) while setting both incident (θ_{in}) and reflection (θ_{ref}) angles to 90 − θ_{view} (θ_{in} = θ_{ref} = 90 − θ_{view}). Reflection spectra measurements for the rocking curves were performed by rocking the sample in both directions (Figure 7a,b). The incident beam angle (θ_{in}) and detection angle (θ_{ref}) with respect to the initial sample position were set in such a way that the angle between the incident beam and the detector (ω) remained unchanged during rocking. When ω = 50°, θ_{in} = θ_{ref} = 65° at 0 rocking angle (ψ). At ψ = 5°, ω = 50° and θ_{in} = 60° while θ_{ref} = 70°.

Tensile Test. Tensile stress−strain properties of both gel sheets and rods were measured with a commercial test machine (Tensilon RTC-1310A, Orientec Co.). Prior to testing, the gel sheets were cut into a dumbbell-shaped standardized size with a gel cutter (JIS-K6251-7) in such a way that the tensile elongation could be performed parallel to the top surface of the gel, that is, in the direction along the lamellae. The gel rods were clamped as is. The distance between the two clamps was considered as the initial length of the gel rod. Deformation was applied along the long axis of the gel rod. The stretching velocity was 200 mm/min for both gels.

■ ASSOCIATED CONTENT

Supporting Information

The Supporting Information is available free of charge on the ACS Publications website at DOI: 10.1021/acsomega.7b01443.

Additional results related to the swelling of the as-prepared gels and reflection spectral analysis for rocking curves (PDF)

Real-time movie taken by a conventional video camera to show the angle-dependent color of the gel sheet (AVI)

Real-time movie taken by a conventional video camera to show the angle-independent color of the gel rod (AVI)

■ AUTHOR INFORMATION

Corresponding Author

*E-mail: gong@sci.hokudai.ac.jp.

ORCID

Md. Anamul Haque: 0000-0002-2461-9532

Takayuki Nonoyama: 0000-0001-8554-0636

Jian Ping Gong: 0000-0003-2228-2750

Notes

The authors declare no competing financial interest.

■ ACKNOWLEDGMENTS

This research was financially supported by a grant-in-aid for Scientific Research (S) (no. 17H06144), Postdoctoral Fellowships for Foreign Researchers (no. 15F15043) of the Japan Society for the Promotion of Science (JSPS), and JSPS KAKENHI grant number JP17H06376. The authors would like to thank Dr. Daniel R. King for his contribution to language presentation throughout the paper.

■ REFERENCES

(1) Hu, Z.; Lu, X.; Gao, J.; Wang, C. Polymer Gel Nanoparticle Networks. *Adv. Mater.* **2000**, *12*, 1173−1176.

(2) Arsenault, A. C.; Puzzo, D. P.; Manners, I.; Ozin, G. A. Photonic-crystal full-colour displays. *Nat. Photonics* **2007**, *1*, 468−472.

(3) Matsubara, K.; Watanabe, M.; Takeoka, Y. A Thermally Adjustable Multicolor Photochromic Hydrogel. *Angew. Chem.* **2007**, *119*, 1718−1722.

(4) Ueno, K.; Matsubara, K.; Watanabe, M.; Takeoka, Y. An Electro- and Thermochromic Hydrogel as a Full-Color Indicator. *Adv. Mater.* **2007**, *19*, 2807−2812.

(5) Nakayama, D.; Takeoka, Y.; Watanabe, M.; Kataoka, K. Simple and Precise Preparation of a Porous Gel for a Colorimetric Glucose Sensor by a Templating Technique. *Angew. Chem., Int. Ed.* **2003**, *42*, 4197−4200.

(6) Holtz, J. H.; Asher, S. A. Polymerized colloidal crystal hydrogel films as intelligent chemical sensing materials. *Nature* **1997**, *389*, 829−832.

(7) Zhang, C.; Losego, M. D.; Braun, P. V. Hydrogel-Based Glucose Sensors: Effects of Phenylboronic Acid Chemical Structure on Response. *Chem. Mater.* **2013**, *25*, 3239−3250.

(8) Takeoka, Y. Angle-independent structural coloured amorphous arrays. *J. Mater. Chem.* **2012**, *22*, 23299−23309.

DOI: 10.1021/acsomega.7b01443
ACS Omega 2018, 3, 55−62

(9) Guidetti, G.; Atifi, S.; Vignolini, S.; Hamad, W. Y. Flexible Photonic Cellulose Nanocrystal Films. *Adv. Mater.* **2016**, *28*, 10042−10047.
(10) Kamita, G.; Frka-Petesic, B.; Allard, A.; Dargaud, M.; King, K.; Dumanli, A. G.; Vignolini, S. Biocompatible and Sustainable Optical Strain Sensors for Large-Area Applications. *Adv. Opt. Mater.* **2016**, *4*, 1950−1954.
(11) Iwayama, Y.; Yamanaka, J.; Takiguchi, Y.; Takasaka, M.; Ito, K.; Shinohara, T.; Sawada, T.; Yonese, M. Optically Tunable Gelled Photonic Crystal Covering Almost the Entire Visible Light Wavelength Region. *Langmuir* **2003**, *19*, 977−980.
(12) Arsenault, A. C.; Clark, T. J.; et al. From colour fingerprinting to the control of photoluminescence in elastic photonic crystals. *Nat. Mater.* **2006**, *5*, 179−184.
(13) Sumioka, K.; Kayashima, H.; Tsutsui, T. Tuning the Optical Properties of Inverse Opal Photonic Crystals by Deformation. *Adv. Mater.* **2002**, *14*, 1284−1286.
(14) Fudouzi, H.; Sawada, T. Photonic Rubber Sheets with Tunable Color by Elastic Deformation. *Langmuir* **2006**, *22*, 1365−1368.
(15) Hu, Z.; Huang, G. A New Route to Crystalline Hydrogels, Guided by a Phase Diagram. *Angew. Chem., Int. Ed.* **2003**, *42*, 4799−4802.
(16) Cai, T.; Wang, G.; Thompson, S.; Marquez, M.; Hu, Z. Photonic Hydrogels with Poly(ethylene glycol) Derivative Colloidal Spheres as Building Blocks. *Macromolecules* **2008**, *41*, 9508−9512.
(17) Matsubara, K.; Watanabe, M.; Takeoka, Y. A Thermally Adjustable Multicolor Photochromic Hydrogel. *Angew. Chem., Int. Ed.* **2007**, *46*, 1688−1692.
(18) Weissman, J. M.; Sunkara, H. B.; Tse, A. S.; Asher, S. A. Thermally Switchable Periodicities and Diffraction from Mesoscopically Ordered Materials. *Science* **1996**, *274*, 959−963.
(19) Lee, Y.-J.; Braun, P. V. Tunable Inverse Opal Hydrogel pH Sensors. *Adv. Mater.* **2003**, *15*, 563−566.
(20) Way, A. E.; Hsu, L.; Shanmuganathan, K.; Weder, C.; Rowan, S. J. pH-Responsive Cellulose Nanocrystal Gels and Nanocomposites. *ACS Macro Lett.* **2012**, *1*, 1001−1006.
(21) Marlow, F.; Muldarisnur; Sharifi, P.; Brinkmann, R.; Mendive, C. Opals: Status and Prospects. *Angew. Chem., Int. Ed.* **2009**, *48*, 6212−6233.
(22) Hu, Z.; Lu, X.; Gao, J. Hydrogel Opals. *Adv. Mater.* **2001**, *13*, 1708−1712.
(23) Zhou, B.; Gao, J.; Hu, Z. Robust polymer gel opals—An easy approach by inter-sphere cross-linking gel nanoparticle assembly in acetone. *Polymer* **2007**, *48*, 2874−2881.
(24) Wang, W.; Zhang, W.; Gu, J.; Liu, Q.; Deng, T.; Zhang, D.; Lin, H.-Q. Design of a structure with low incident and viewing angle dependence inspired by Morpho butterflies. *Sci. Rep.* **2013**, *3*, 3427.
(25) Kolle, M.; Lethbridge, A.; Kreysing, M.; Baumberg, J. J.; Aizenberg, J.; Vukusic, P. Bio-Inspired Band-Gap Tunable Elastic Optical Multilayer Fibers. *Adv. Mater.* **2013**, *25*, 2239−2245.
(26) Dong, W. J.; Lo, N.-T.; Jung, G. H.; Ham, J.; Lee, J.-L. Efficiency enhancement and angle-dependent color change in see-through organic photovoltaics using distributed Bragg reflectors. *Appl. Phys. Lett.* **2016**, *108*, 103902.
(27) Si, G.; Zhao, Y.; Leong, E. S. P.; Lv, J.; Liu, Y. J. Incident-angle dependent color tuning from a single plasmonic chip. *Nanotechnology* **2014**, *25*, 455203.
(28) Takeoka, Y.; Honda, M.; Seki, T.; Ishii, M.; Nakamura, H. Structural Colored Liquid Membrane without Angle Dependence. *ACS Appl. Mater. Interfaces* **2009**, *1*, 982−986.
(29) Harun-Ur-Rashid, M.; Imran, A. B.; Seki, T.; Ishii, M.; Nakamura, H.; Takeoka, Y. Angle-Independent Structural Color in Colloidal Amorphous Arrays. *ChemPhysChem* **2010**, *11*, 579−583.
(30) Gotoh, Y.; Suzuki, H.; Kumano, N.; Seki, T.; Katagiri, K.; Takeoka, Y. An amorphous array of poly(N-isopropylacrylamide) brush-coated silica particles for thermally tunable angle-independent photonic band gap materials. *New J. Chem.* **2012**, *36*, 2171−2175.
(31) Marlow, F.; Muldarisnur; Sharifi, P.; Brinkmann, R.; Mendive, C. Opals: Status and Prospects. *Angew. Chem., Int. Ed.* **2009**, *48*, 6212−6233.
(32) Kang, Y.; Walish, J. J.; Gorishnyy, T.; Thomas, E. L. Broad-wavelength-range chemically tunable block-copolymer photonic gels. *Nat. Mater.* **2007**, *6*, 957−960.
(33) Stavenga, D. G.; Wilts, B. D.; Leertouwer, H. L.; Hariyama, T. Polarized iridescence of the multilayered elytra of the Japanese jewel beetle, Chrysochroa fulgidissima. *Philos. Trans. R. Soc., B* **2011**, *366*, 709−723.
(34) Haque, M. A.; Kamita, G.; Kurokawa, T.; Tsujii, K.; Gong, J. P. Unidirectional Alignment of Lamellar Bilayer in Hydrogel: One-Dimensional Swelling, Anisotropic Modulus, and Stress/Strain Tunable Structural Color. *Adv. Mater.* **2010**, *22*, 5110−5114.
(35) Haque, M. A.; Kurokawa, T.; Kamita, G.; Yue, Y.; Gong, J. P. Rapid and Reversible Tuning of Structural Color of a Hydrogel over the Entire Visible Spectrum by Mechanical Stimulation. *Chem. Mater.* **2011**, *23*, 5200−5207.
(36) Mito, K.; Haque, M. A.; Nakajima, T.; Uchiumi, M.; Kurokawa, T.; Nonoyama, T.; Gong, J. P. Supramolecular hydrogels with multi-cylindrical lamellar bilayers: Swelling-induced contraction and anisotropic molecular diffusion. *Polymer* **2017**, *128*, 373−378.
(37) Yue, Y. F.; Haque, M. A.; Kurokawa, T.; Nakajima, T.; Gong, J. P. Lamellar Hydrogels with High Toughness and Ternary Tunable Photonic Stop-Band. *Adv. Mater.* **2013**, *25*, 3106−3110.
(38) Yue, Y.; Kurokawa, T.; Haque, M. A.; Nakajima, T.; Nonoyama, T.; Li, X.; Kajiwara, I.; Gong, J. P. Mechano-actuated ultrafast full-colour switching in layered photonic hydrogels. *Nat. Commun.* **2014**, *5*, 4659.
(39) Haque, M. A.; Kurokawa, T.; Gong, J. P. Anisotropic hydrogel based on bilayers: color, strength, toughness, and fatigue resistance. *Soft Matter* **2012**, *8*, 8008−8016.
(40) Li, X.; Kurokawa, T.; Takahashi, R.; Haque, M. A.; Yue, Y.; Nakajima, T.; Gong, J. P. Polymer Adsorbed Bilayer Membranes Form Self-Healing Hydrogels with Tunable Superstructure. *Macromolecules* **2015**, *48*, 2277−2282.
(41) Naitoh, K.; Ishii, Y.; Tsujii, K. Iridescent Phenomena and Polymerization Behaviors of Amphiphilic Monomers in Lamellar Liquid Crystalline Phase. *J. Phys. Chem.* **1991**, *95*, 7915.
(42) Ghoshal, A.; DeMartini, D. G.; Eck, E.; Morse, D. E. Experimental determination of refractive index of condensed reflectin in squid iridocytes. *J. R. Soc., Interface* **2014**, *11*, 20140106.
(43) Zhou, C.; Heath, D. E.; Sharif, A. R. M.; Rayatpisheh, S.; Oh, B. H. L.; Rong, X.; Beuerman, R.; Chan-Park, M. B. High Water Content Hydrogel With Super High Refractive Index. *Macromol. Biosci.* **2013**, *13*, 1485−1491.
(44) Vukusic, P. Evolutionary Photonics with a Twist. *Science* **2009**, *325*, 398−399.
(45) Sharma, V.; Crne, M.; Park, J. O.; Srinivasarao, M. Structural origin of circularly polarized iridescence in jeweled beetles. *Science* **2009**, *325*, 449−451.
(46) Vukusic, P.; Sambles, J. R. Photonic structures in biology. *Nature* **2003**, *424*, 852−855.
(47) Bragg, W. H.; Bragg, W. L. The Reflection of X-rays by Crystals. *Proc. R. Soc. London, Ser. A* **1913**, *88*, 428−438.
(48) Myers, H. P. *Introductory Solid State Physics*; CRC Press, Taylor & Francis, 2002; Chapter 3, pp 48−52.
(49) Chen, X.; Mayama, H.; Matsuo, G.; Torimoto, T.; Ohtani, B.; Tsujii, K. Effect of ionic surfactants on the iridescent color in lamellar liquid crystalline phase of a nonionic surfactant. *J. Colloid Interface Sci.* **2007**, *305*, 308−314.

DOI: 10.1021/acsomega.7b01443
ACS Omega 2018, 3, 55−62